Naval Research Laboratory
Washington, DC 20375-5320

NRL/6360/MR—2023/2

Tuning the Functionality of Materials with Reversible Phase Transitions

HEUNGSOO KIM
RAYMOND C.Y. AUYEUNG

Materials and Systems Branch
Materials Science and Technology Division

ALBERTO PIQUÉ

Materials and Sensors Branch
Materials Science and Technology Division

January 26, 2023

REPORT DOCUMENTATION PAGE

Form Approved
OMB No. 0704-0188

1. REPORT DATE *(DD-MM-YYYY)*	**2. REPORT TYPE**	**3. DATES COVERED** *(From - To)*
23-01-2023	NRL Memorandum Report	October 1, 2017 – September 30, 2022

4. TITLE AND SUBTITLE

Tuning the Functionality of Materials with Reversible Phase Transitions

5a. CONTRACT NUMBER

5b. GRANT NUMBER

5c. PROGRAM ELEMENT NUMBER

6. AUTHOR(S)

Heungsoo Kim, Raymond C.Y. Auyeung, and Alberto Piqué

5d. PROJECT NUMBER

5e. TASK NUMBER

5f. WORK UNIT NUMBER
1J42

7. PERFORMING ORGANIZATION NAME(S) AND ADDRESS(ES)

Naval Research Laboratory
4555 Overlook Avenue, SW
Washington, DC 20375-5320

8. PERFORMING ORGANIZATION REPORT NUMBER

NRL/6360/MR--2023/2

9. SPONSORING / MONITORING AGENCY NAME(S) AND ADDRESS(ES)

Naval Research Laboratory
4555 Overlook Avenue, SW
Washington, DC 20375-5320

10. SPONSOR / MONITOR'S ACRONYM(S)

NRL

11. SPONSOR / MONITOR'S REPORT NUMBER(S)

12. DISTRIBUTION / AVAILABILITY STATEMENT

DISTRIBUTION STATEMENT A: Approved for public release; distribution is unlimited.

13. SUPPLEMENTARY NOTES

14. ABSTRACT

We investigated solid-state phase transitions of complex metal oxides as an effective way to dynamically control macroscopic material properties and their functionality via lattice and defect engineering. We demonstrated that careful film growth and the strain generated by buffer layers can provide an effective way for tuning the transition temperature of metal oxides with reversible phase transitions such as VO2 films and in the process control their functionality. We also demonstrated an ultrafast switching capability (<400 fs) of the strained VO2 films using a time-resolved optoelectronic autocorrelation measurement technique, indicating that it is possible to selectively activate the metallic phase without inducing the associated structural transition. Furthermore, to demonstrate the applicability of this basic research, we fabricated VO2-based, layered solid-state radiators for spacecraft thermal control. The multilayer radiators in this work are well suited for spacecraft thermal control because they are passive and self-regulating. We also demonstrated that perovskite conducting oxides can provide a large tunable permittivity in the mid-wave IR (MWIR) range (2-7 μm) for MWIR plasmonic devices. These results are highly relevant to various Navy and DoD applications ranging from optical communications to low observables. Lastly, we were able to synthesize two different structural phases of epitaxial Ti2O3 films. The films grown at 485 °C are a corundum structure with p-type carriers while the films grown at 730 °C become an orthorhombic structure with n-type carriers. These results can open up the possibility of p-n homojunctions that will strongly impact future Navy and DoD applications including IR detection and thermal energy conversion.

15. SUBJECT TERMS

16. SECURITY CLASSIFICATION OF:			**17. LIMITATION OF ABSTRACT**	**18. NUMBER OF PAGES**	**19a. NAME OF RESPONSIBLE PERSON**
					Heungsoo Kim
a. REPORT	**b. ABSTRACT**	**c. THIS PAGE**	U	21	**19b. TELEPHONE NUMBER** *(include area code)*
U	U	U			(202) 404-2094

Standard Form 298 (Rev. 8-98)
Prescribed by ANSI Std. Z39.18

This page intentionally left blank.

Tuning the Functionality of Materials with Reversible Phase Transitions

Heungsoo Kim, Ray Auyeung, Alberto Piqué

Materials and Systems Branch
Materials Science and Technology Division

Abstract

We investigated solid-state phase transitions of complex metal oxides as an effective way to dynamically control macroscopic material properties and their functionality via lattice and defect engineering. We demonstrated that careful film growth and the strain generated by buffer layers can provide an effective way for tuning the transition temperature of metal oxides with reversible phase transitions such as VO_2 films and in the process control their functionality. We also demonstrated an ultrafast switching capability (<400 fs) of the strained VO_2 films using a time-resolved optoelectronic autocorrelation measurement technique, indicating that it is possible to selectively activate the metallic phase without inducing the associated structural transition. Furthermore, to demonstrate the applicability of this basic research, we fabricated VO_2-based, layered solid-state radiators for spacecraft thermal control. The multilayer radiators in this work are well suited for spacecraft thermal control because they are passive and self-regulating. We also demonstrated that perovskite conducting oxides can provide a large tunable permittivity in the mid-wave IR (MWIR) range (2-7 μm) for MWIR plasmonic devices. These results are highly relevant to various Navy and DoD applications ranging from optical communications to low observables. Lastly, we were able to synthesize two different structural phases of epitaxial Ti_2O_3 films. The films grown at 485 °C are a corundum structure with p-type carriers while the films grown at 730 °C become an orthorhombic structure with n-type carriers. These results can open up the possibility of p-n homojunctions that will strongly impact future Navy and DoD applications including IR detection and thermal energy conversion.

Introduction

We present here the closeout report on our program, *Tuning the Functionality of Materials with Reversible Phase Transitions*, WU# 1J42. This program aimed to control solid-state phase transitions of complex metal oxides as mechanisms to dynamically adjust macroscopic material properties via investigation of the role of lattice structure, electrical and optical properties. Reversible solid-state phase transitions present a unique method to tune a wide range of functionalities such as electrical and thermal conductivity, magnetic susceptibility, dielectric polarizability and optical properties. This is in stark contrast to current material systems, which require non-reversible changes in composition or processing in order to adjust the above properties. Recently, both the number of materials and the range of applications for materials with reversible phase transformations have expanded significantly [1-4]. The ability to vary the crystal structure or the electron band configuration through the influence of an external magnetic, electric or strain field paves the way towards new functionality and applications.

Manuscript approved January 26, 2023.

A significant outcome of this work as described below has been the study of novel, emergent phenomena in complex metal oxide thin films with strongly interacting electronic, optic and lattice degrees of freedom. We investigated several material systems including VO_2, La-doped $BaSnO_3$, Sn-doped In_2O_3 (ITO) and Ti_2O_3 that exhibit novel properties in regions of the electromagnetic spectrum that are less explored, i.e. long wave IR (LWIR) and mid-wave IR (MWIR) [5-13]. These material systems were selected such that they provide a means to dynamically control electrical and optical properties. We focused on determining the underlying physical mechanisms of tunability, corelating electrical behavior and material properties in the systems, and evaluating fundamental performance limits for Naval applications. This research will provide material systems that will strongly impact future Navy and other DoD development of new types of low power, low loss RF switches, dynamic apertures for sensor tunability and protection (RF to visible), and new types of monolithically integrated optical and electrical sensors. At the end of this report, we also provide a list of publications (23 papers including two book chapters), presentations (20 presentations including 10 invited and 10 contributed) and patent (1) generated from the results achieved under this program.

Use of buffer layer to control the metal-to-insulator transition temperature (T_{MIT}) of VO_2

The first material system in this program was vanadium dioxide (VO_2). VO_2 undergoes a metal-insulator transition (MIT) at ~68 ˚C, which is associated with a structural phase transition (SPT) between an insulating monoclinic phase and a metallic tetragonal phase when it is triggered by thermal, electrical, or optical stimuli. This SPT leads to a sharp conductivity change by several orders of magnitude. Adjusting the MIT temperature (T_{MIT}) is advantageous from a device standpoint as it allows for the tuning of the device properties. Doping with high-valence metal ions into the VO_2 lattice is a commonly used method to achieve tuning of the T_{MIT} in VO_2 films. However, increasing doping level in VO_2 films generally leads to either a reduction in the magnitude of the transition or broadening of the transition width. Previously, the reduced T_{MIT} was achieved by suppressing the structural transition in ultrathin epitaxially strained VO_2 films (<10 nm) grown on lattice-matched TiO_2 substrates. However, ultrathin VO_2 films are difficult to manufacture due to the easy oxidation to V_2O_5 during the device fabrication process, limiting further applications. In addition, the films become relaxed as they are grown thicker (>10 nm), leading to an increase in the transition temperature. To overcome the strain relaxation issue in thicker VO_2 films, we utilized *buffer layers* to provide an additional degree of freedom to control the strain in thicker VO_2 films.

The first buffer layer we investigated was a tin dioxide (SnO_2), which functions as an excellent buffer because it has the same tetragonal crystal structure and space group as metallic VO_2 (P42/mnm). We have successfully deposited epitaxial VO_2/SnO_2 thin film heterostructures on m-cut sapphire substrates by pulsed laser deposition (PLD). By adjusting the growth conditions of the SnO_2 buffer layers (~150 nm), we were able to control the interfacial strain between VO_2 and SnO_2 buffer layer such that the T_{MIT} of the VO_2 films can be reduced from 68 ˚C to 52 ˚C without diminishing the magnitude or sharpness of their transition. It is shown that in-plane tensile strain and out-of-plane compressive strain of the VO_2 films lead to a decrease of T_{MIT}. Additionally, x-ray diffraction data shows that the VO_2 films grown on SnO_2 buffered Al_2O_3 suppress the monoclinic-VO_2 phase, inducing a structural phase transition from tetragonal-like VO_2 to tetragonal VO_2 during the transition. These results suggest that the strain generated by the SnO_2 buffer provides an effective way for tuning the T_{MIT} of VO_2 films. In summary, the

combination of growing thicker films and the suppression of the structural transition will help reduce resistive losses while maintaining sub-picosecond switching times (Figure 1).

RuO_2 was also proposed as a functional buffer because it has the same crystal structure and space group as both TiO_2 and metallic VO_2 and at the same time allows the fabrication of out-of-plane thin-film-based devices. For example, the RuO_2 buffer layer can be used as a bottom oxide electrode for VO_2 based devices with out-of-plane configurations, considerably reducing the switching voltage and current required for operation as compared with VO_2-based planar type devices. Epitaxial VO_2 thin films were deposited on conductive RuO_2/TiO_2 templates by PLD. The MIT temperature (T_{MIT}) of $VO_2/RuO_2/TiO_2$ heterostructures can be tuned from 59 ˚C to 24 ˚C by adjusting the strain state of the films by decreasing the RuO_2 thickness from 50 nm to 10 nm. For comparison, the sheet resistance curves of 100 nm VO_2 films on TiO_2 substrates with and without the RuO_2 buffer layer are plotted in the same figure (Fig. 4c). Without the RuO_2 buffer layer, the T_{MIT} of the VO_2 film increases from 30 ˚C to 60 ˚C. The boundaries between RuO_2 structures are favorable regions responsible for the nucleation of dislocations, which can partially relieve the strain in the film, thereby sustaining intermediate strain states even with large thicknesses (~100 nm). This allows lowering of the T_{MIT} to near room temperature. These results suggest that the strain generated by the RuO_2 buffer layer can provide an effective way for tuning the T_{MIT} of VO_2 films and provide a route to realizing out-of-plane electrical switching devices (Figure 2).

Ultrafast transition dynamics in strained VO_2 films

Understanding the dynamic conductivity in VO_2 is of critical importance for both understanding the insulator-metal phase transition (IMT) physics and developing next generation configurable photonic devices. An ultrafast optoelectronic autocorrelation technique was used to directly measure the dynamical electrical properties of epitaxially strained VO_2 across the IMT. Strained and fully relaxed epitaxial films of VO_2 were produced by PLD utilizing different substrates and film thickness: 8 nm thick VO_2 on (001) TiO_2 and 60 nm thick VO_2 on (001) Al_2O_3 substrates. Both strained and fully relaxed films exhibit abrupt change in resistivity, indicating the IMT in each. By tailoring the film growth conditions, film thickness and substrate selection, various strain states can be exploited to reduce the IMT temperature to values ranging between 20 – 80°C [Fig. 3(a)].

We measured the dynamical resistivity using this optoelectronic autocorrelation technique on strained epitaxial films of VO_2 on TiO_2 (001) substrates [Fig.3(b)]. Our approach differs from purely optical methods, such as pump–probe measurements, where electrical properties of the material must be inferred from reflected or transmitted light. While the optoelectronic autocorrelation technique uses a combination of optical excitation and electrical sensing, the method differs significantly from purely electrical VO_2 switching measurements that use high amplitude voltage pulses to initiate the IMT. Purely electrical switching experiments have a relatively low temporal resolution due to the electrical readout, which is typically limited to nanosecond time scales. In contrast to the strain-relaxed VO_2 films on c-cut Al_2O_3, the resistance evolution of the strained VO_2 exhibits an ultrafast response that shows switching of the material to the metallic phase, and a return to the insulating state, lasting < 400 fs [Fig. 3(c)]. This short time scale limits the possibility of a structural change in the VO_2, which typically persists for nanoseconds after ultrafast optical excitation of the IMT. These results suggest that a selective excitation of the IMT is possible and support recent findings indicating the structural component of the

phase transition can be suppressed in epitaxially strained VO_2 films. These findings are particularly relevant for developing optical and optoelectronic devices for applications that require fast, high-contrast switching.

VO_2-based radiators for spacecraft thermal control

Building upon the knowledge gained earlier in the program on the growth of VO_2, we fabricated a multilayered solid-state radiator for spacecraft thermal control, as a demonstration of the applicability of this basic research. The ability to grow continuous high quality VO_2 thin film heterostructures enabled us to experimentally demonstrate a passive radiator for thermal control in a simulated space environment. Two VO_2-based radiator designs were demonstrated during this program for spacecraft thermal control applications.

The first radiator design was based on an inverted multilayer structure. In this design, the VO_2-based thermal radiator, which consisted of a BaF_2 dielectric spacer sandwiched between a VO_2 layer and an Au reflecting layer, achieved passive and switchable thermal emissivity control based on the VO_2 phase transition. By shifting the IR transparent Si substrate to the front of the window, the Si can then shield the multilayer thin film structure from the external environment, including exposure to atomic oxygen flux resulting in much improved device lifetimes. This new approach enabled the fabrication of high-quality thermal radiators for spacecraft applications much less likely to fail due to strain from thermal coefficient mismatch between layers or due to damage from exposure in outer space. When the VO_2 layer was in an insulating state at $T< 340$ K, the multilayer structure behaved like a simple infrared reflector, thereby minimizing radiative heat loss. However, when the VO_2 layer switched to a metallic state at $T > 340$ K, the multilayer structure behaved like a resonant absorber with high emissivity in the mid-infrared region (8-12 μm), thus providing a radiative cooling effect. A quantitative comparison between the emitted power using normal and hemispherical emissivity was performed. The radiator showed an excellent emissivity contrast of $\Delta\varepsilon \sim 0.47$ comparable with previously published results using the normal emissivity values. However, using normal emissivity values leads to an overestimate of actual performance because it does not consider the angular dependence of the multilayer radiator design. While the measured hemispherical emissivity change of the radiator was $\Delta\varepsilon \sim 0.35$, the experimentally measured radiated power increases by more than a factor 7 with a net radiated power difference of 480 W/m^2 between 300 K and 373 K (Figure 4).

The second radiator design was VO_2-based radiators using mechanically stable TiN and Al_2O_3 layers. In this design, the layered thin-film radiator consists of a TiN bottom infrared mirror, an Al_2O_3 dielectric spacer and a VO_2 top absorber layer to achieve dynamic thermal emissivity for spacecraft thermal control application. First, an analytical modeling approach was used to optimize the optical response of the layered radiators by varying the thickness of Al_2O_3 spacers and VO_2 layers for maximum emissivity change ($\Delta\varepsilon$) between 25 ºC and 80 ºC. The results of this simulations showed that the thin-film radiators composed of the optimized thickness of VO_2 (30 – 50 nm) and Al_2O_3 (600 – 800 nm) can provide the highest emissivity change ($\Delta\varepsilon \sim 0.48$) between these two temperature states. Experimental results validated the simulations for a radiator with a 50 nm thick VO_2 layer and a 600 nm of Al_2O_3 layer which exhibited a maximum emissivity change ($\Delta\varepsilon \sim 0.46$) under the same temperature range. Our

experimental results agree very well with the modeling results obtained from the same radiator design. These results are of crucial importance for designing mechanically and thermally stable radiators for spacecraft thermal control due to the stability of both TiN and Al_2O_3 materials. The multilayer radiators in this work are well suited for spacecraft thermal control because they are passive and self-regulating (Figure 5).

Transparent conducting perovskite oxides for Near-IR (NIR) and Mid-IR (MIR) plasmonics

The second material system in this program was La-doped $BaSnO_3$ (LBSO). We focused on growth of epitaxial LBSO thin films that can serve as a transparent electrode for studying ferroelectric transitions in perovskite films, such as $BaTiO_3$. We deposited epitaxial LBSO thin films by PLD on two different substrates ($SrTiO_3$ and MgO). As a result of this work we were able to tune the permittivity over a mid-infrared range (2 μm to 6 μm) that enables the use of LBSO films as an electrically conducting, optically transparent buffer layer for active phase change based infrared plasmonic devices.

First, we completed our study on the epitaxial growth of LBSO thin films on (001) $SrTiO_3$ substrates by PLD. Specifically, we studied the tunable permittivity of La-doped $BaSnO_3$ (LBSO) epitaxial films in the mid-infrared range. By adjusting the oxygen pressure and substrate temperature during deposition, we were able to control the film crystallinity and strain, which modified the electrical and optical properties of the LBSO films. The LBSO films grown at an oxygen pressure of 100 mTorr and a growth temperature of 780 ˚C show the highest conductivity (3.6×10^3 S cm^{-1}) with a carrier concentration of 3.5×10^{20} cm^{-3} and a carrier mobility of 65 $cm^2V^{-1}s^{-1}$. The observed high conductivity corresponds to the film with the best crystallinity and the lowest strain (<0.2 %) state. The permittivity of the LBSO films can also be tuned as a function of the oxygen pressure and temperature during deposition allowing tuning their epsilon-near-zero (ENZ) wavelength from 2 μm to 5.6 μm (Figure 6).

In contrast to the LBSO films grown on perovskite $SrTiO_3$ substrates, we also investigated epitaxial LBSO films on non-perovskite MgO substrates. MgO was selected due to its low dielectric constant, which is much more efficient for electro-optic modulators operating at microwave frequencies. We were able to control the film crystallinity and strain by changing the oxygen partial pressure during deposition, which in turn enabled modifying the electrical and optical properties of the films. The LBSO films grown at oxygen pressures of 100 mTorr show reduced strain and low resistivity (4.4×10^{-4} Ω-cm), while the films grown at 10 mTorr of oxygen show increased strain and high resistivity (8.2×10^{-2} Ω-cm). Optical properties of the LBSO films were also adjusted by varying the oxygen deposition pressure. The average transmittance in the visible range is greater than 70% for both films. The optical band gap of the LBSO films increased from 3.81 eV to 3.87 eV with increasing oxygen deposition pressure from 10 mTorr to 100 mTorr. The permittivity of the LBSO films was modified as a function of the oxygen pressure during deposition allowing tuning their epsilon-near-zero (ENZ) wavelength from 2.2 μm to 7 μm. This large tunable permittivity in the mid-IR range makes LBSO films strong candidates as an electrically conducting, optically transparent buffer layer for MIR plasmonic devices that are highly relevant to various Navy and DoD applications ranging from optical communications to low observables (Figure 7).

Ti_2O_3 films

The third material system studied was Ti_2O_3. Unlike VO_2 or V_2O_3 phase changing materials, Ti_2O_3 shows the metal-insulator transition (MIT) electronically without a structural phase transition. Thus, the timescale of the electronic MIT in Ti_2O_3 can be much faster than the MIT induced by the structural changes (such as VO_2), resulting in ultrafast switching responses to the external stimuli. These unique properties can be used in switching devices for numerous applications, including IR detection and thermal energy conversion. We deposited Ti_2O_3 thin films on single crystal *c*-Al_2O_3 substrates via PLD. No additional processing gases were introduced during growth to maintain low pressure and eliminate oxygen from the system. Ti_2O_3 films were grown at both 485°C and 730°C resulting in two different structural phases. The resulting films, grown at different temperatures, were determined to have different carrier types, with the low temperature (LT) film (485°C) being p-type and the higher temperature (HT) film (730°C) being n-type. The ability to grow Ti_2O_3 films with different carrier types opens up the possibility for p-n homojunctions. (Figure 8).

Furthermore, the XRD and Raman data indicated that the LT-Ti_2O_3 films had an elongated c-axis and the electrical and optical measurements demonstrated that these films showed metallic conduction that did not transition to insulating at any temperature. At room temperature, the optical conductivity of these films matched that of the bulk high temperature metallic Ti_2O_3 as did the position of the Raman A_{1g} mode. This indicated that our film was strain-locked in the metallic state at all temperatures. A likely explanation for this lattice deformation is due to the grain structure of the films. In Ti_2O_3 nanoparticles, it has been reported that there is an increase in the c-axis and a decrease in the a-axis length as the nanoparticle size is reduced. The grain size in our films is approximately 15 – 33 nm, which should yield a (c/a) ratio of ~2.69 based on the previous results on Ti_2O_3 nanoparticles. This is consistent with our observed c/a ratio of 2.7. In bulk Ti_2O_3, this c/a ratio occurred at T ~550 K, well into the metallic state.

From our data it is clear that our films were strained to a metallic (c/a) ratio at room temperature due to the grain size causing local c-axis elongation and a-axis contraction. This local strain was preventing the shorting of the c-axis to a point where the Ti^{3+}–Ti^{3+} dimers can fully isolate to a $a_{1g}a_{1g}^{*}$ singlet while also keeping the a-axis contracted to allow the conduction along the a-b plane through the $e_g{}^{\pi}$ band. This grain size induced strain locks the film into a metallic state and prevents the bandgap from opening at all temperatures. (Figure 9).

Laser surface structuring of metal oxide thin films

We have studied laser induced crystallization and surface structuring of metal oxide thin films. In contrast to the use of epitaxial strain where the strain is set by the lattice constants at the unit cell level, laser induced crystallization and surface structuring allow for spatially varying morphologies and access to thermodynamic conditions that are outside of conventional growth techniques. Rather than relying on conventional excimer laser-based crystallization methods, we investigated the coherent interference of two pulsed laser beams, also referred to as direct laser interference pattering (DLIP). This technique allows for control of the spatial period by adjusting the interference angle. We demonstrated highly ordered linear crystallization in indium tin oxide (ITO) thin films, which yielded a spatial period of 650 nm. Furthermore, unlike DLIP, a single laser beam can also produce periodic patterns with sub-

micrometer feature sizes, also referred to as laser-induced periodic surface structures (LIPSS). We were able to produce the LIPSS structure (a period of 75 nm) on the ITO films (Figure 10).

We utilized a UV picosecond laser pulses to produce simultaneous DLIP and LIPSS features in a single laser step on ITO films (~150 nm). Results show that the DLIP formation is more dominant than the LIPSS formation when high laser fluences were applied, while the LIPSS formation is dominant at low fluences. By utilizing optimized laser conditions (laser polarization, fluence, number of laser pulses, pulse duration) of a picosecond laser system, we were able to produce both LIPSS and DLIP structures of the ITO films. The combination of picosecond laser pulses and interfering beams allowed for hierarchical patterning in ITO thin films with feature sizes spanning two orders of magnitude, from 75 nm up to 50 µm, which is the size of the laser spot. After laser patterning, the ITO thin films exhibited an anisotropic electrical resistance of 50,000:1 and a strong polarization contrast in the LWIR (Figure 10).

Future Plans

Perovskite oxides such as $BaTiO_3$ have become attractive materials to extend the functionalities of silicon-based photonics platforms due to their large Pockels coefficient (> 1000 pm/V). For example, $BaTiO_3$-based integrated photonics potentially provide a wide spectral operating range (visible to mid-IR), higher power handling, rapid frequency tunability, low linear losses and nonlinear behavior. The epitaxial film growth and defect/ strain engineering approaches developed under this WU led to a new program (WU# 1AC4: Functional Materials for Integrated Photonics) that will identify the basic material properties of the perovskite oxides as new functional materials for integrated photonics for broadband application (UV to SWIR). In addition, we plan to pursue further research on other oxide systems including thermochromic VO_2, phase transition Ti_2O_3 and perovskite conducting oxides for improving their functionality in various applications under WU# 1AC4.

Figures

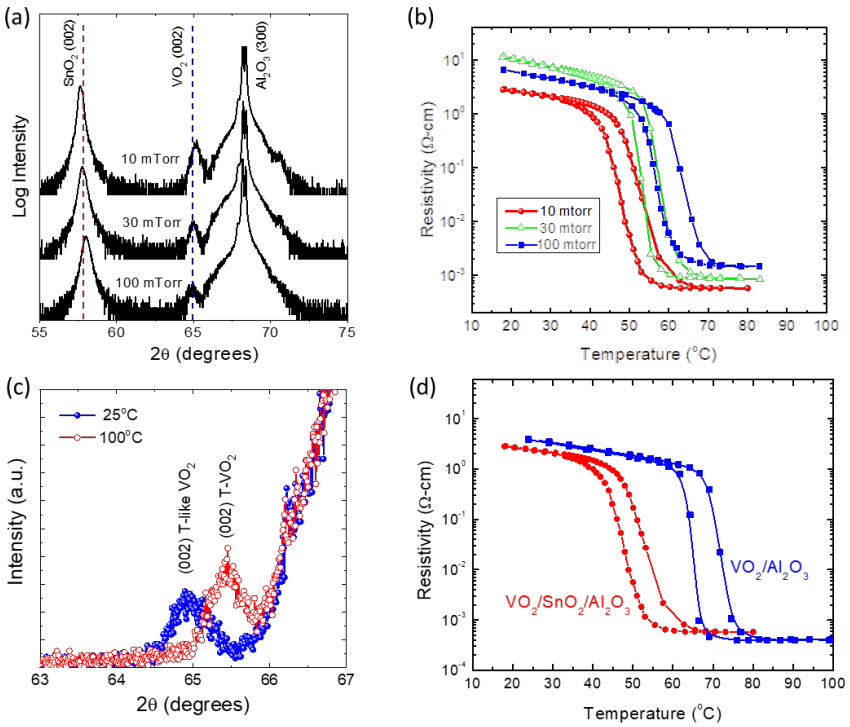

Figure 1. (a) θ-2θ XRD scans and (b) electrical resistivity vs temperature of VO_2/SnO_2 thin films (~50 nm) grown on m-cut sapphire substrates, where the SnO_2 buffer layers were grown at various oxygen pressures (10-100 mTorr). The red broken line represents the bulk SnO_2 (002) peak position and the blue broken line represents the bulk VO_2 (002) peak position in (a). (c) Temperature-dependent θ-2θ XRD scans of VO_2 film on 30 mTorr SnO_2/Al_2O_3 buffer layer at 25 ºC and 100 ºC. (d) Electrical resistivity vs temperature for 50 nm VO_2 film on SnO_2/Al_2O_3 (red) and 50 nm VO_2 film on Al_2O_3 (blue). [Adapted from Ref. 5].

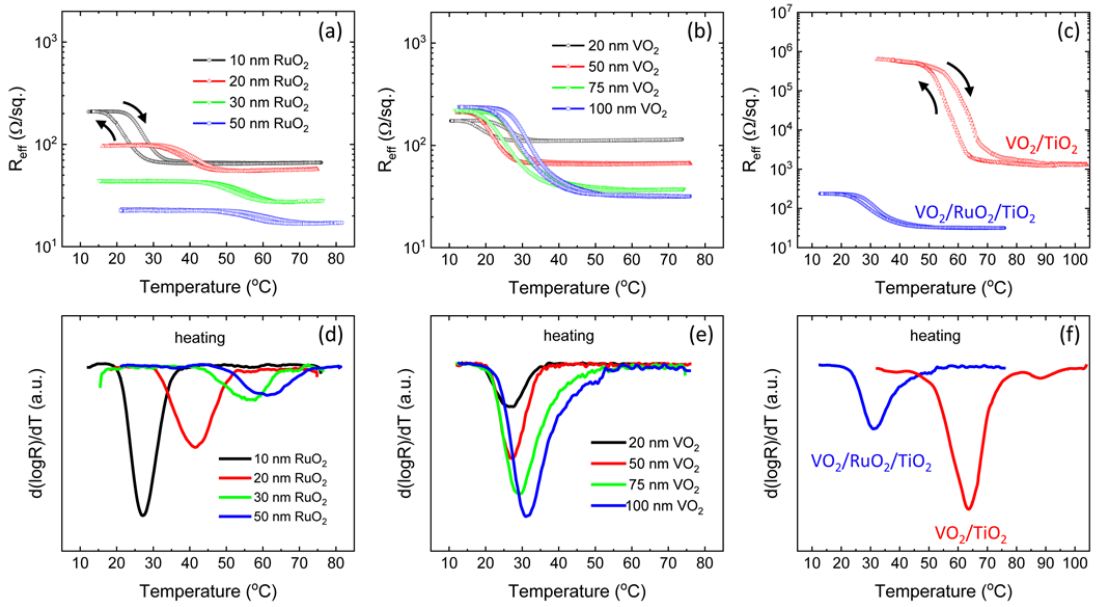

Figure 2. (a) Effective sheet resistance vs temperature for 50 nm thick VO_2 films grown on RuO_2/TiO_2 as a function of RuO_2 buffer layer thickness (10 – 50 nm). (b) Effective sheet resistance vs temperature for various thicknesses of VO_2 films (20, 50, 75 and 100 nm) grown on RuO_2 (10 nm)/TiO_2 templates. (c) Effective sheet resistance vs temperature for 100 nm VO_2 films grown on TiO_2 substrates with /without RuO_2 buffer layer. Arrows show measurement direction. (d) - (f) Corresponding derivative curves during heating process for plots in (a), (b) and (c), respectively. [Adapted from Ref. 6].

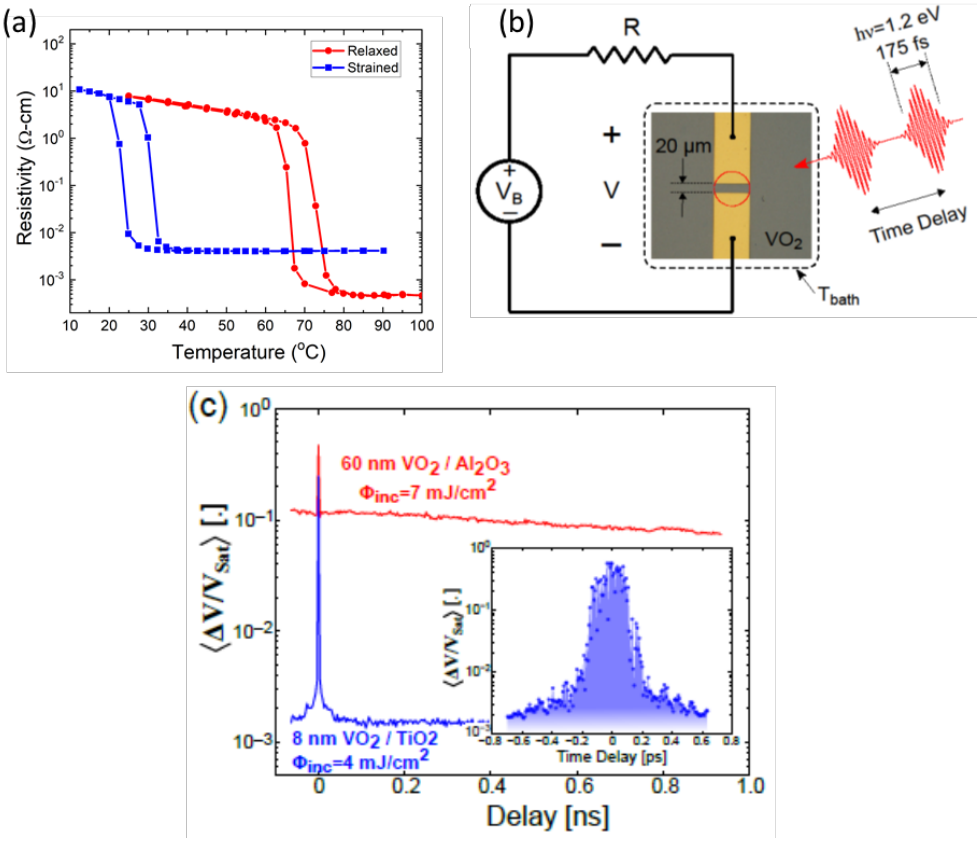

Figure 3. Resistivity of relaxed (red) and strained (blue) VO2 films as a function of temperature. (b) Schematic showing the autocorrelation measurement and an optical micrograph of the VO2 channel formed between two gold contacts. (c) Average normalized change in voltage across the VO2 channel plotted as a function of time delay for strained (blue) and relaxed (red) films. The inset shows detail of the strained film response around zero-time delay. [Adapted from Ref. 7].

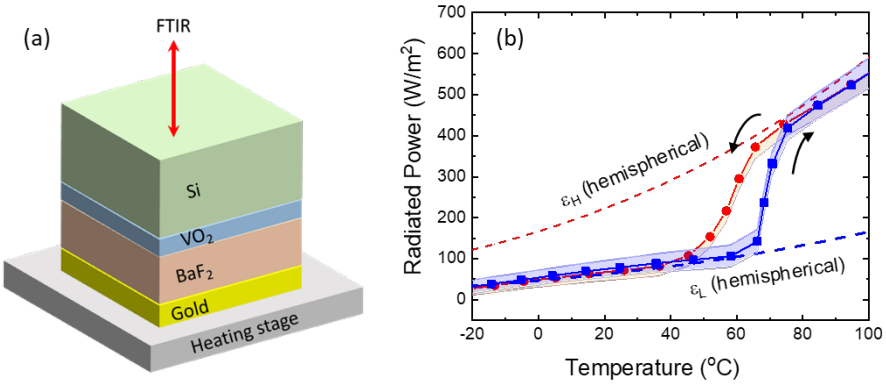

Figure 4. (a) Schematic illustration of the multilayer structure mounted upside down to the temperature-controlled stage inside an FTIR microscope. (b) Radiated thermal power of a multilayer structure with a 60 nm thick VO_2 layer. The direction of heating and cooling are indicated by arrows. [Adapted from Ref. 8].

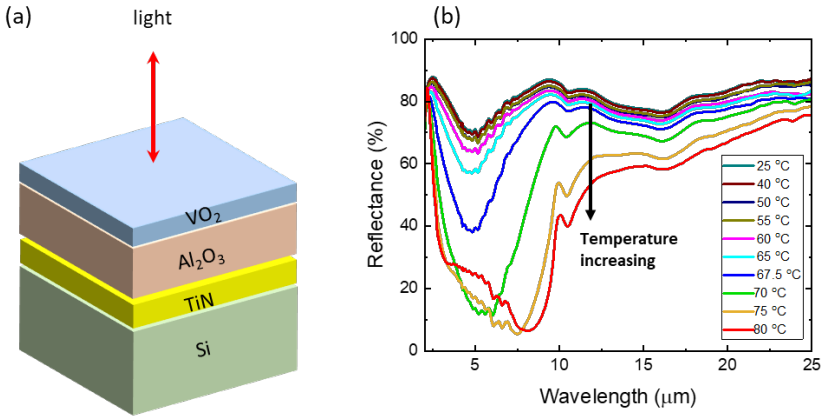

Figure 5. (a) Schematic illustration of the thermal radiator. (b Experimental reflectance spectra of VO_2-based multilayer structures at various temperatures from 25°C to 80 °C during heating. The thickness of VO_2, Al_2O_3, and TiN layers is 50 nm, 600 nm and 70 nm, respectively. [Adapted from Ref. 9].

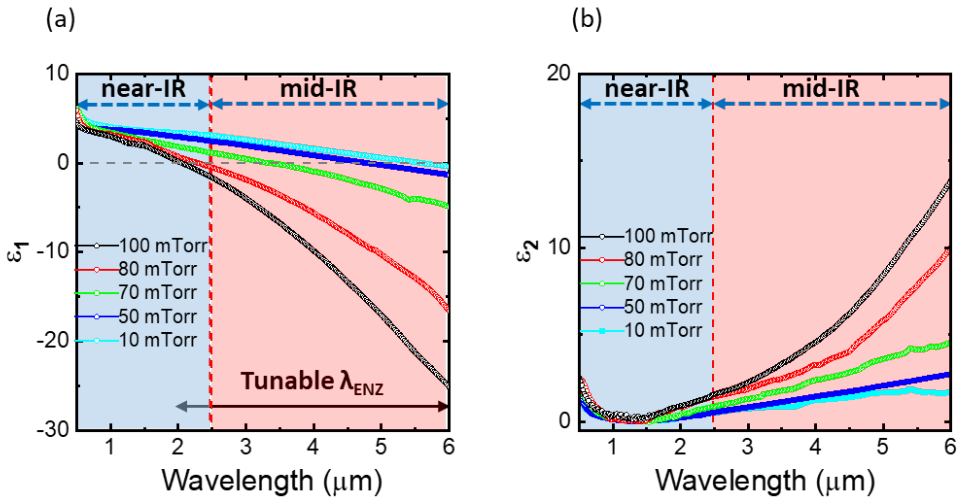

Figure 6. (a) Real (ε_1) and (b) imaginary (ε_2) parts of permittivity of 100 nm thick La-doped $BaSnO_3$ (LBSO) films deposited on $SrTiO_3$ substrates at various oxygen pressures (10 - 100 mTorr). The permittivity of the LBSO films can be tuned as a function of the oxygen pressure allowing tuning their epsilon-near-zero (ENZ) wavelength from 2 μm to 5.6 μm. [Adapted from Ref. 10].

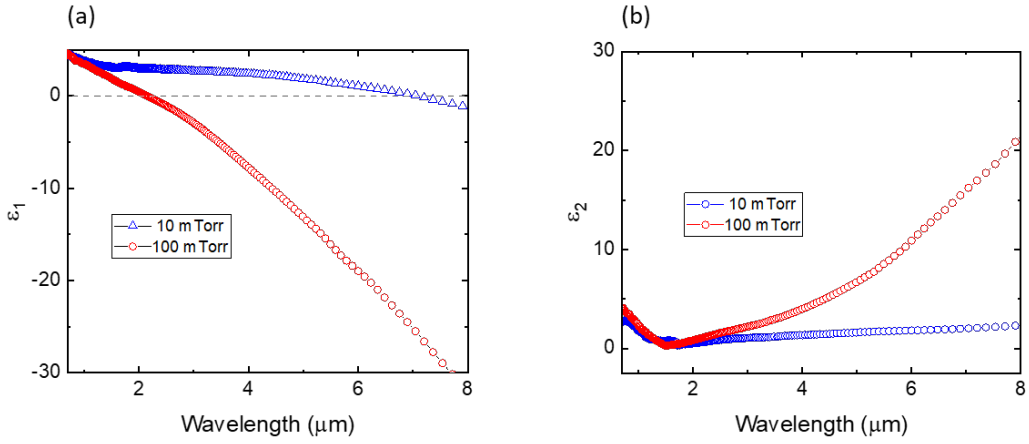

Figure 7. (a) Real (ε_1) and (b) imaginary (ε_2) parts of permittivity of 100 nm thick La-doped $BaSnO_3$ (LBSO) films deposited on MgO substrates at two different oxygen pressures (10 and 100 mTorr). The permittivity of the LBSO films can be tuned as a function of the oxygen pressure allowing tuning their ENZ wavelength from 2 μm to 7 μm. [Adapted from Ref. 11].

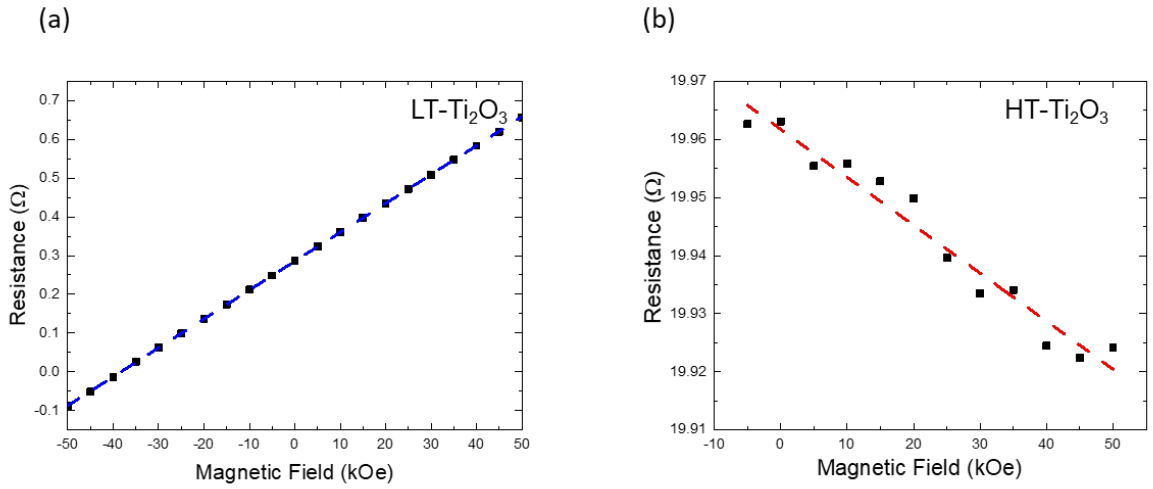

Figure 8. Resistance vs magnetic field of Ti2O3 films grown at two different temperatures: (a) 485 °C (LT) and (b) 730 °C (HT). LT-Ti_2O_3 film yields trigonal (corundum) *p*-type film, while. HT-Ti_2O_3 film yields an orthorhombic *n*-type film.

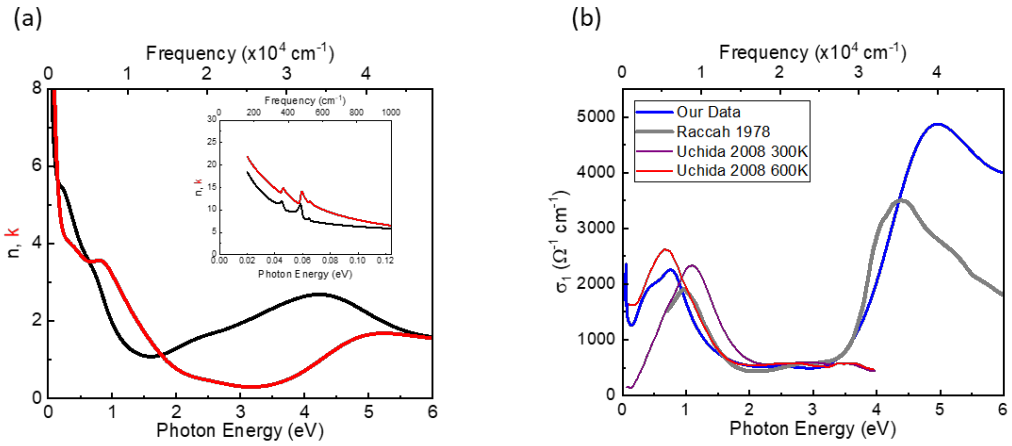

Figure 9. (a) Optical constants (n, k) and (b) broadband optical conductivity of 140nm LT-Ti_2O_3 films deposited on c-Al_2O_3 substrate at 485 °C. Inset in (a) shows the zoomed in region in the far infrared showing the Drude feature from free carrier contributions. [Adapted from Ref. 12].

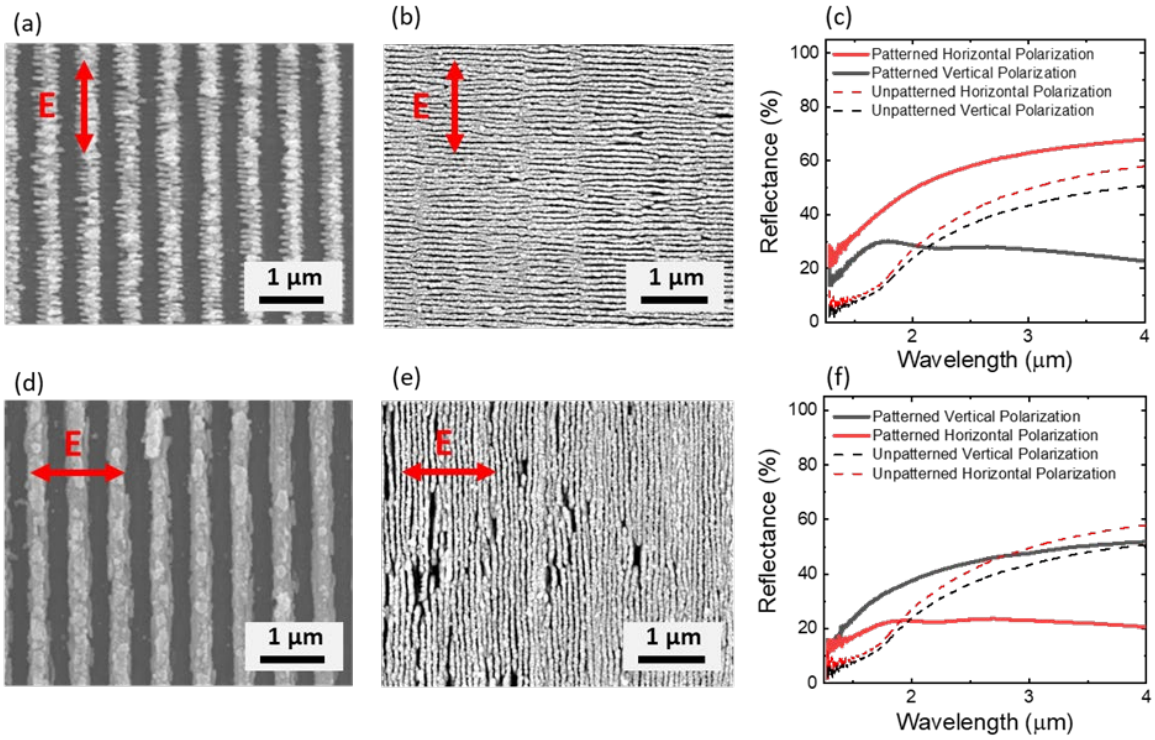

Figure 10. SEM images showing combination of LIPSS and DLIP structures in ITO films irradiated with (a,d) an intermediate laser fluence (90 mJ/cm^2, 200 kHz and 5 mm/s) and (b,e) a low laser fluence (32 mJ/cm^2, 500 kHz and 0.1 mm/s) with an electric field parallel (a,b) and perpendicular (d,e) to the DLIP. (c,f) Polarized infrared reflectance of laser-structured ITO films with (b) horizontal and (e) vertical LIPSS structures. [Adapted from Ref. 13].

Publications

1. (Journal) H. Kim, N.S. Bingham, N.A. Charipar, A. Piqué, "Strain effect in epitaxial VO2 thin films grown on sapphire substrates using SnO2 buffer layers," *AIP Advances* 7, 105116 (2017). doi: 10.1063/1.5004125. (17-1231-4053).

2. (Journal) K.M. Charipar, N.A. Charipar, J.C. Prestigiacomo, N.S. Bingham, A. Piqué, "Laser printing of flip-chip interconnects for high frequency applications," *Journal of Manufacturing Processes* 32, 110-115 (2018). doi: 10.1016/j.jmapro.2018.01.019. (18-1231-0142).

3. (Conf Proc) K.M. Charipar, R.E. Diaz-Rivera, N.A. Charipar, A. Piqué, "Laser-induced forward transfer (LIFT) of 3D microstructures," SPIE Proc. 10523, Laser 3D Manufacturing V (2018). doi: 10.1117/12.2294578. (18-1231-0334).

4. (Conf Proc) Y. Xiao, N.A. Charipar, A. Piqué, M. Kats, "Ultrafast pulse generation in the mid-infrared via modulated emissivity," CLEO JW2A.121, (2018). doi: 10.1364/CLEO_AT.2018.JW2A.121. (18-1231-4679).

5. (Conf Proc) Y. Xiao, N.A. Charipar, A. Piqué, M. Kats, "Nanosecond Mid-Infrared Pulse Generation Via Modulated Thermal Emission," 2018 IEEE Research & Applications of Photonics in Defense (RAPID) ThC3.4, (2018). (18-1231-1413).

6. (Conf Proc) R.J. Suess, P. Johns, J. Naciri, N.A. Charipar, J. Fontana, "Welding dynamics of plasmonic gold nanorods under femtosecond laser excitation," CLEO SM2O.1, (2018). doi:10.1364/CLEO_SI.2018.SM2O.1. (18-1231-0046).

7. (Conf Proc) A. Piqué, H. Kim, R.J. Suess, K.M. Charipar, R.C.Y. Auyeung, N.S. Bingham, N. Charipar, "Tunable metamaterials based on the metal-insulator transition in vanadium oxide," Advanced Photonics Congress NoTh2D.3, (2018). doi: 10.1364/NOMA.2018.NoTh2D.3. (18-1231-1009).

8. (Journal) P. Serra, A. Piqué, "Laser-induced forward transfer: fundamentals and applications," Adv. Mater. Technol. **4**,1800099 (2019). doi: 10.1002/admt.201800099. (18-1231-1111).

9. (Journal) N. Charipar, R.C.Y. Auyeung, H. Kim, K. Charipar, A. Piqué, "Hierarchical patterning in indium tin oxide thin films," Optical Materials Express, 9 (7), 3035-3045 (2019). doi: 10.1364/OME.9.003035. (19-1231-1701).

10. (Journal) H. Kim, N.A. Charipar, J. Figueroa, N.S. Bingham, A. Piqué, "Control of metal-insulator transition temperature of VO2 thin films grown on RuO2/TiO2 templates by strain modification," AIP Advances, 9 (1), 015302 (2019). doi: 10.1063/1.5083848. (18-1231-4584).

11. (Journal) H. Kim, K. Cheung, R.C.Y. Auyeung, D.E. Wilson, K.M. Charipar, A. Piqué, N.A. Charipar, "VO2-based switchable radiator for spacecraft thermal control," Scientific Reports, 9, 11329 (2019). doi: 10.1038/s41598-019-47572-z. (18-1231-4629).

12. (Journal) Y. Xiao, N.A. Charipar, J. Salman, A. Piqué, M.A. Kats, "Nanosecond mid-infrared pulse generation via modulated thermal emissivity," Light: Science & Applications, 8 (1), 51 (2019). doi:10.1038/s41377-019-0158-6. (18-1231-4475).

13. (Conf Proc) K.M. Charipar, R.E. Diaz-Rivera, N.H. DeJesus-Villanueva, R.C.Y. Auyeung, N.A. Charipar, A. Piqué, "Reusable laser-absorbing layers for LIFT," SPIE Proc. 10905, Laser Applications in Microelectronic and Optoelectronic Manufacturing (LAMOM XXIV) (2019). doi: 10.1117/12.2513012. (19-1231-0213).

14. (Book Chapter) A. Piqué, K. M. Charipar, Laser-Induced Forward Transfer Processes in Additive Manufacturing, Additive Manufacturing Processes, V. 24, ASM Handbook, Edited by David L. Bourell, William Frazier, Howard Kuhn, Mohsen Seifi, ASM International, p 446–455 (2020). https://doi.org/10.31399/asm.hb.v24.a0006565. (19-1231-3375).

15. (Book Chapter) A. Piqué and K.M. Charipar, "Laser-induced Forward Transfer (LIFT)," in Handbook of Laser Micro- and Nano-Engineering, ed. Koji Sugioka, Springer (2020). https://doi.org/10.1007/978-3-319-69537-2_26-1. (20-1231-0710).

16. (Journal) K. Charipar, H. Kim, A. Piqué, N. Charipar, "ZnO Nanoparticle/Graphene Hybrid Photodetectors via Laser Fragmentation in Liquid," Nanomaterials 10 (9), 1648 (2020). doi: 10.3390/nano10091648. (NRL/JA/20-1231-1650).

17. (Journal) H. Kim, N.A. Charipar, A. Piqué, "Tunable permittivity of La-doped BaSnO3 thin films for near- and mid-infrared plasmonics," Journal of Physics D: Applied Physics 53, 365103 (2020). doi: 10.1088/1361-6463/ab91ed. (20-1231-1123).

18. (Conf Proc) H. Kim, N.A. Charipar, R.C.Y. Auyeung, K.M. Charipar, A. Piqué, "Laser processing of plasmonic metal oxides and phase change materials, Proc. SPIE 11268, 1126816 (2020). doi: 10.1117/12.2546933. (19-1231-3375). (20-1231-0420).

19. (Conf Proc) N.A. Charipar, H. Kim, K.M. Charipar, A. Piqué, "Applications of Graphene as a Transparent Conductor," NATO AVT-304 RSM on Graphene Technologies and Applications for Defense Proceedings, STO-MP-AVT-304 (2020). doi: 10.14339/STO-MP-AVT-304-14-PDF. (19-1231-2289).

20. (Journal) N. Charipar, H. Kim, K.M. Charipar, A. Piqué, "Graphene-based Ultraviolet Photodetectors Using Zinc Oxide Thin Films," Journal of NATO Science and Technology Organization: Applied Vehicle Technology Panel, 2, 67-76 (2020). (20-1231-1645).

21. (Conf Proc) H. Kim, N.A. Charipar, R.C.Y. Auyeung, K.M. Charipar, A. Piqué, "La-doped BaSnO3 films for mid-infrared plasmonic applications," Proc. SPIE **11687**, Oxide-based Materials and Devices XII, 168712 (2021). doi: 10.1117/12.2578946. (IR-6364-21-9-U).

22. (Journal) H. Kim, D. Lahneman, C. Rohde, and A. Piqué, "VO2-based thin-film radiators with variable thermal emissivity," Thin Sold Films 759, 139455 (2022). doi.org/10.1016/j.tsf.2022.139455. (IR-6364-22-9-U).

23. (Journal) D. J. Lahneman, H. Kim, H. Jiang, S.A. Mathews, E. Lock, J. Prestigiacomo, M.M. Qazilbash, C. Rohde, and A. Piqué, "Electronic and optical properties of strain-locked metallic Ti2O3 films," Curr. Appl. Phys. 47, 9-14 (2023). doi.org/10.1016/j.cap.2022.12.006. (IR-6364-22-12-U).

Patents

1. J. Fontana, J. Naciri, B. Ratna, N. Charipar, A. Piqué, Optical applications of nanosphere metasurfaces, U.S Patent # 10,280,310, issued May 7, 2019.

Presentations

1. "Optoelectronic applications of vanadium dioxide," N.A. Charipar, R.J. Suess, H. Kim, K. Charipar, S. Mathews, R.C.Y. Auyeung, A. Piqué, Advanced Laser Technologies (ALT2018), Sept. 9th – 14th 2018, Tarragona, Spain. (18-1231-2285) (Invited)

2. “Laser-induced forward transfer for electronics packaging,” N.A. Charipar, R. Auyeung, H. Kim, K. Charipar, S. Mathews, A. Piqué, 30th Electronics Packaging Symposium, Sept. 19th 2018, Binghamton, NY. (18-1231-3161) (Invited)

3. “Laser-induced forward transfer techniques for printing functional materials,” H. Kim, R. Auyeung, N. Charipar, S. Mathews, K. Charipar, A. Piqué, Frontiers in Lasers and Applications (FLA 2018), April 16th – 19th 2018, Okinawa, Japan. (17-1231-4428) (Invited)

4. “Laser tuned plasmonic metasurfaces,” University of Barcelona Seminar, Sept. 14th 2018, Barcelona, Spain,” N.A. Charipar, H. Kim, J. Geldmeier, S. Trammell, K. Charipar, J. Naciri, R.J. Suess, A. Piqué, J. Fontana, University of Barcelona Seminar, Sept. 14th 2018, Barcelona, Spain (18-1231-2719) (Invited)

5. “Using laser direct-write for 3D printing functional devices,” A. Piqué, SPIE Security + Defense, Sept. 10th – 13th 2018, Berlin, Germany. (18-1231-2575) (Invited)

6. “Laser patterning of plasmonic metasurfaces,” N.A. Charipar, H. Kim, J. Geldmeier, S. Trammell, K.M. Charipar, J. Naciri, R. Suess, A. Piqué, J. Fontana, Laser Precision Microfabrication (LPM2018), June 25th – 29th 2018, Edinburgh, Scotland, UK. (18-1231-1584)

7. “Tunable metamaterials based on the metal-insulator transition in vanadium oxide,” A. Piqué, H. Kim, R.J. Suess, K.M. Charipar, R.C.Y. Auyeung, N.S. Bingham, N. Charipar, OSA Advanced Photonics Congress July 2-5, 2018, Zurich, Switzerland. (18-1231-1609) (Invited)

8. “Reusable laser-absorbing layers for LIFT,” K.M. Charipar, R.E. Diaz-Rivera, N.H. DeJesus-Villanueva, R.C.Y. Auyeung, N.A. Charipar, A. Piqué, SPIE Photonics West, February 3-7, 2019, San Francisco, CA. STRN:NRL/OP/6360/19/731.

9. “Phase transition-based Terahertz and Infrared Devices,” N.A. Charipar, H. Kim, R. Auyeung, S. Mathews, K. Charipar, A. Piqué, Advances in Functional Materials Conference, July 24th, 2019, Washington, DC. (18-1231-2338) STRN:NRL/AO/6360/19/325 (Invited)

10. “Control of metal-insulator transition temperature in VO2 thin films by strain modification via various buffer layers,” H. Kim, N.A. Charipar, A. Piqué, Advances in Functional Materials Conference, July 24th, 2019, Washington, DC. (18-1231-2337) STRN:NRL/AO/6360/19/326

11. “Laser Processing of Self-Assembled Plasmonic Metasurfaces,” N. Charipar, H. Kim, J. Geldmeier, S. Trammell, K. Charipar, J. Naciri, A. Piqué, J. Fontana, Laser Precision Microfabrication (LPM2019), May 21th – 24th 2019, Hiroshima, Japan. (19-1231-1169) (Invited)

12. “Current progress and future opportunities in Laser-induced Forward Transfer (LIFT),” A. Piqué, 15th Int’l. Conference on Laser Ablation (COLA 2019), Sept. 12th, 2019, Maui, Hawaii. (19-1231-2104) (Invited)

13. “LIFT of Microstructures Using Elastomeric Donor Templates,” K.M. Charipar, R.C.Y. Auyeung, H. Kim, N.A. Charipar, A. Piqué, Laser Precision Microfabrication (LPM2019), May 21th – 24th 2019, Hiroshima, Japan. (19-1231-1079)

14. “Applications of Graphene as a Transparent Conductor,” N.A. Charipar, H. Kim, K.M. Charipar, A. Piqué, NATO AVT-304 Specialist Meeting on Graphene Technique & Applications for Defense, 10-11th October 2019, Trondheim, Norway. (19-1231-3064)

15. “Laser processing of plasmonic metal oxides and phase change materials,” H. Kim, N.A. Charipar, R.C.Y. Auyeung, K.M. Charipar, A. Piqué, SPIE Photonics West 2020, Laser-based Micro- and Nanoprocessing XIV, Feb. 5th 2020, San Francisco, CA. (20-1231-0233) (Invited)

16. “Laser Processing of Titanium: Oxide Formation for Electronic Applications,” K. Charipar, C. Musi, H. Kim, R. Auyeung, A. Piqué, N. Charipar, SPIE Photonics West 2020, LAMOM XXV, Feb. 4th 2020, San Francisco, CA. (20-1231-0133). STRN:NRL/OP/6360/20/018

17. “Multi-scale Laser Processing of Thin Oxide Films,” N.A. Charipar, R.C.Y. Auyeung, H. Kim, K.M. Charipar, A. Piqué, 21st International Symposium on Laser Precision Microfabrication 2020 (LPM2020), June 23 2020, Dresden, Germany (attended virtually). STRN: NRL/6360/20/200.

18. “Laser-based Fabrication of ZnO/Graphene Hybrid Photodetectors,” K. Charipar, H. Kim, A. Piqué, N. Charipar, 21st International Symposium on Laser Precision Microfabrication 2020 (LPM2020), June 23 2020, Dresden, Germany (attended virtually). STRN: NRL/6360/20/199.

19. “La-doped $BaSnO_3$ films for near- and mid-infrared plasmonic applications,” H. Kim, N.A. Charipar, R.C.Y. Auyeung, K.M. Charipar, A. Piqué, SPIE Photonics West 2021, March 2021, San Francisco, CA (attended virtually). STRN: NRL/6360/ON--2021/4.

20. “Control of phase transition of VO2 films and VO2-based terahertz and infrared devices,” H. Kim, D. Lahneman, R. Auyeung, K. Charipar, C. Rhode[1] and A. Piqué, *ICMCTF* conference in San Diego, May 22-25 (2022). STRN: NRL/6360/ON—2022/16

References

1. Z. Shao, X. Cao, H. Luo and P. Jin, “Recent progress in the phase-transition mechanism and modulation of vanadium dioxide materials,” NPG Asia Materials **10**, 581-605 (2018).

2. K. Liu, S. Lee, S. Yang, O. Delaire, J. Wu, “Recent progresses on physics and applications of vanadium dioxide,” Materials Today **21**, 875-896 (2018).

3. J. Zhang and R.D. Averitt, “Dynamics and control in complex transition metal oxides,” Annu. Rev. Mater. Res., **44**, 19-43 (2014).

4. Z. Yang, C. Ko, and S. Ramanathan, “Oxide Electronics Utilizing Ultrafast Metal-Insulator Transitions,” Annu. Rev. Mater. Res. **41**, 337–67 (2011).

5. H. Kim, N.S. Bingham, N.A. Charipar, A. Piqué, “Strain effect in epitaxial VO2 thin films grown on sapphire substrates using SnO2 buffer layers,” AIP Advances **7**, 105116 (2017).

6. H. Kim, N.A. Charipar, J. Figueroa, N.S. Bingham, A. Piqué, “Control of metal-insulator transition temperature of VO2 thin films grown on RuO2/TiO2 templates by strain modification,” AIP Advances **9** (1), 015302 (2019).

7. R.J. Suess, N.S. Bingham, K.M. Charipar, H. Kim, S.A. Mathews, A. Piqué, N.A. Charipar, “Ultrafast Phase Transition Dynamics in Strained Vanadium Dioxide Films,” *Adv. Mater. Interfaces 1700810, 1-6* (2017).

8. H. Kim, K. Cheung, R.C.Y. Auyeung, D.E. Wilson, K.M. Charipar, A. Piqué, N.A. Charipar, “VO2-based switchable radiator for spacecraft thermal control,” Scientific Reports **9**, 11329 (2019).

9. H. Kim, D. Lahneman, C. Rohde, and A. Piqué, “VO2-based thin-film radiators with variable thermal emissivity,” Thin Sold Films **759**, 139455 (2022).

10. H. Kim, N.A. Charipar, A. Piqué, “Tunable permittivity of La-doped BaSnO3 thin films for near- and mid-infrared plasmonics,” Journal of Physics D: Applied Physics **53**, 365103 (2020).

11. H. Kim, N.A. Charipar, R.C.Y. Auyeung, K.M. Charipar, A. Piqué, “La-doped BaSnO3 films for mid-infrared plasmonic applications,” Proc. SPIE **11687**, Oxide-based Materials and Devices XII, 168712 (2021).

12. D. J. Lahneman, H. Kim, H. Jiang, S.A. Mathews, E. Lock, J. Prestigiacomo, M.M. Qazilbash, C. Rohde, and A. Piqué, “Electronic and optical properties of strain-locked metallic Ti2O3 films,” Curr. Appl. Phys. **47**, 9-14 (2023).

13. N. Charipar, R.C.Y. Auyeung, H. Kim, K. Charipar, A. Piqué, “Hierarchical patterning in indium tin oxide thin films,” Optical Materials Express **9** (7), 3035-3045 (2019).